IEEE Access
Multidisciplinary | Rapid Review | Open Access Journal

Received February 22, 2018, accepted March 30, 2018, date of publication April 10, 2018, date of current version May 2, 2018.

Digital Object Identifier 10.1109/ACCESS.2018.2825283

Synchronization of Chemical Reaction Networks Based on DNA Strand Displacement Circuits

CHENGYE ZOU[1], XIAOPENG WEI[1], QIANG ZHANG[1, 2], AND YUAN LIU[1]
[1]School of Computer Science and Technology, Dalian University of Technology, Dalian 116024, China
[2]Key Laboratory of Advanced and Intelligent Computing, Ministry of Education, Dalian University, Dalian 116622, China

Corresponding authors: Xiaopeng Wei (xpwei@dlu.cn) and Qiang Zhang (zhangq@dlut.edu.cn)

This work was supported in part by the National Natural Science Foundation of China under Grant 61425002, Grant 61751203, and Grant 61772100, in part by the Program for Changjiang Scholars and Innovative Research Team in University under Grant IRT_15R07, and in part by the Program for Liaoning Innovative Research Team in University under Grant LT2015002.

ABSTRACT Reversible bimolecular chemical reactions are elementary chemical reactions. This paper investigated this reaction type based on DNA strand displacement, and proposed degradation, catalysis, and annihilation reactions along with the synchronization reaction modules. DNA reaction modules were compared with ideal reaction modules, and relative reaction rates analyzed using the Lotka–Volterra oscillator as an example to demonstrate the validity of these reaction modules. An arbitrary chemical reaction network was employed to numerically simulate and predict synchronization between two Lotka–Volterra oscillators.

INDEX TERMS DNA strand displacement, Lotka–Volterra oscillator, reaction networks, projective synchronization.

I. INTRODUCTION

Digital and analog DNA circuits based on DNA strand displacement (DSD) have advanced significantly due to their modularity, programmability, and versatility, but their design and control is difficult due to nonlinearities and uncertainties in reaction networks. Reaction modules are useful for DNA circuit control. Current DNA reaction modules incorporate degradation, annihilation, catalysis, integration, gain, and summation reaction modules. Oishi et al. investigated DNA reaction modules for biomolecular implementation of linear I/O systems [12]. Yordanov et al. proposed a computational design of nucleic acid feedback control circuits through DNA reaction modules [13]. Soloveichik et al. used DNA reaction modules to realize many classical models, including Lotka-Volterra oscillators, oregonators, and Rössler chaotic systems [14].

Synchronization as an important dynamical behavior, and has attracted considerable attention due to potential applications in secure communication, image encryption, chemical reaction networks (CRNs), etc. [15]–[23]. Synchronization is closely relevant for biomedical engineering. For example, Zhou et al. applied synchronization to build responsive DNA nanostructures [24], and Halicka utilized cell synchronization for DNA damage response [25].

Projective synchronization is extension of complete synchronization [27]–[30], and several extended projective synchronization methods have been proposed recently, including function projective synchronization, modified function projective synchronization, and modified projective synchronization. In projective synchronization, drive and response systems are synchronize up to a scaling factor, and the scaling factor is represented the proportionality between the drive (or master) and the response (or slave) system. Potential of projective synchronization in secure communications due to its faster communication, projective synchronization can be used to extend binary digital to M-nary digital communication.

This paper introduces synchronization and projective synchronization to DNA CRNs, because synchronization may offer the replication of DNA strand a new technical means [26], and the realization of synchronization and projective synchronization in digital and analog DNA circuits is of more extensive application potential. Furthermore, the application of synchronization in CRNs is meaningful for investigation of relationship between ideal formal CRNs and DNA CRNs, and complexity and nonlinearity of DNA CRNs.

In this article, we have firstly proved the error degradation of two species by ideal formal or proposed DNA reversible reaction, and investigated influencing factors of speed of degradation. We then introduced this proposed reversible reaction to synchronize two species, extending CRN

synchronization to indirect and multiple synchronizations, and applied this strategy to projective synchronization.

Degradation, catalysis, annihilation reactions and synchronization reaction modules are proposed in our design, and the relationship of reaction rates between DNA and ideal formal CRNs is analyzed. An arbitrary CRN was employed to numerically simulate synchronization and projective synchronization of a Lotka-Volterra oscillator to validate the proposed method.

II. CHEMICAL REACTION MECHANISM OF SYNCHRONIZATION

A. ERROR DEGRADATION OF TWO CHEMICAL SPECIES

Reaction (1a) is a reversible, bimolecular reaction, the DSD implementation of Reaction (1a) is shown by Fig. 1. Let chemical reactants X and Y be two chemical species from different CRNs, and chemical species A and B are auxiliary species, that participate in a reversible, bimolecular reaction,

$$X + A \underset{k2}{\overset{k_1}{\rightleftarrows}} Y + B, \tag{1a}$$

with corresponding ideal formal chemical reaction

$$X \underset{\lambda 2}{\overset{\lambda_1}{\rightleftarrows}} Y, \tag{1b}$$

where k_1 and λ_1 denote the forward, and k_2 and λ_2 denote the backward reaction rate, satisfying

$$\lambda_1 = C_m k_1$$

and

$$\lambda_2 = C_m k_2.$$

Let $[X]_0$, $[Y]_0$, $[A]_0$, and $[B]_0$ represent the initial concentrations of X, Y, A, and B respectively, where

$$C_m = [A]_0 = [B]_0 \gg [X]_0, [Y]_0.$$

It is obvious that, the reaction effect on concentration of A and B can be ignorable. In this article, it is assumed as

$$[A]_0 = [A]_t = [A]$$
$$[B]_0 = [B]_t = [B]$$

The absolute error among X and Y is defined as

$$|[e]_t| = |[X]_t - [Y]_t|, \tag{2}$$

Definition 1: Error of two different chemical species will be degradative, if following are satisfied

$$\begin{cases} k_1 [X]_0 [A] - k_2 [Y]_0 [B] \geq 0 \geq k_1[A] - k_2[B], [X]_0 \geq [Y]_0 \\ k_1 [X]_0 [A] - k_2 [Y]_0 [B] < 0 < k_1[A] - k_2[B], [Y]_0 > [X]_0 \end{cases} \tag{3}$$

Proof 1: When $[X]_0 > [Y]_0$,

$$\begin{cases} \dfrac{d[X]_t}{dt} = k_2 [Y]_t [B] - k_1 [X]_t [A] < 0 \\ \dfrac{d[Y]_t}{dt} = k_1 [X]_t [A] - k_2 [Y]_t [B] > 0 \end{cases} \tag{4}$$

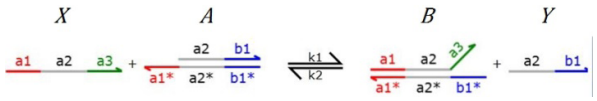

FIGURE 1. The arrow in a DNA strand indicates the 3′ end. The domain a_2 is 12 nucleotides, and the toehold domain is usually less than 10 nucleotides, so the toehold binding reaction is reversible.

The forward reaction trend is stronger than the back reaction trend in (1), and X reacts with A to produce Y and B, and time derivative of absolute error is

$$\begin{aligned} \frac{d|[e]_t|}{dt} &= \frac{d([X]_t - [Y]_t)}{dt} \\ &= 2k_2 [Y]_t [B] - 2k_1 [X]_t [A] \\ &\leq 2k_2 [Y]_\infty [B] - 2k_1 [X]_\infty [A] = 0 \end{aligned} \tag{5}$$

As shown in Figs. 2(a) and 2(c), if curves of X and Y approach equilibrium before intersection, the error among X and Y can be degradative, we have $[X]_\infty > ([X]_0 + [Y]_0)/2$ and $[Y]_\infty < ([X]_0 + [Y]_0)/2$; otherwise curves of X and Y approach equilibrium after intersection, and the error among X and Y can't be degradative as Fig. 2(b) shown.

Thus, in the case as Figs. 2(a) and 2(c) shown, exist

$$\begin{aligned} \frac{d|[e]_\infty|}{dt} &= 2k_2 [Y]_\infty [B] - 2k_1 [X]_\infty [A] \\ &\leq 2k_2 \frac{[X]_0 + [Y]_0}{2} [B] - 2k_1 \frac{[X]_0 + [Y]_0}{2} [A] \\ &= 2\frac{[X]_0 + [Y]_0}{2} (k_2[B] - k_1[A]) \end{aligned} \tag{6}$$

i.e.,

$$k_1 [A] - k_2 [B] \leq 0 \tag{7}$$

where $k_1 [A]$ is crucial to error degradation speed, as shown in Fig. 2. Error degradation in Fig. 2(a) is faster than Fig. 2(b), but concentration of X in Fig. 2(b) is closer to Y than in Fig. 2(a), due to the longer degradation interval.

When $[X]_0 > [Y]_0$, the proof is similar to proof 1, and $k_2 [B]$ is crucial to the error degradation speed.

B. COMPLETE SYNCHRONIZATION OF TWO CHEMICAL SPECIES

Complete synchronization of two CRNs is a special case of degradation as shown by Fig. 3. To show synchronization of two different chemical species, the error between two chemical species is defined as

$$[e]_t = [X]_t - [Y]_t, \tag{8}$$

Definition 2. If $k_1[A] = k_2[B]$ exists, complete synchronization between two different chemical species can be achieved,

where

$$[X]_\infty = [Y]_\infty = ([X]_0 + [Y]_0)/2. \tag{9}$$

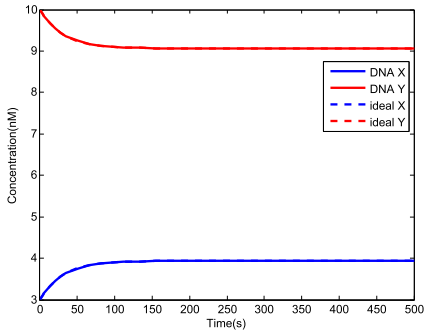

(a)

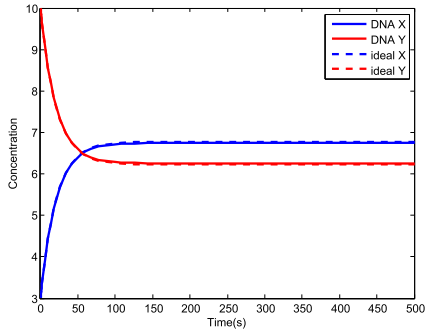

(b)

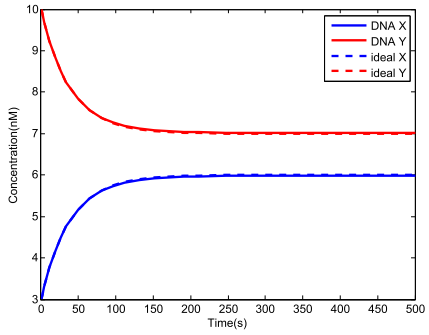

(c)

FIGURE 2. Evolution of X and Y (a) With error degradation: $[X]_0 = 3$nM, $[Y]_0 = 10$nM; $[A]_0 = 10^3$nM, $[B]_0 = 10^3$nM; $k_1 = 2.3 \times 10^{-5}$/nM/s, $k_2 = 1 \times 10^{-5}$/nM/s. (b) Without error degradation: $[X]_0 = 3$nM, $[Y]_0 = 10$nM; $[A]_0 = 10^3$nM, $[B]_0 = 35$nM; $k_1 = 2 \times 10^{-5}$/nM/s, $k_2 = 2.5 \times 10^{-5}$/nM/s. (c) With error degradation: $[X]_0 = 3$nM, $[Y]_0 = 10$nM; $[A]_0 = 10^3$nM, $[B]_0 = 10^3$nM; $k_1 = 1.4 \times 10^{-5}$/nM/s, $k_2 = 1.2 \times 10^{-5}$/nM/s.

Proof 2: Error evolution can be expressed as

$$\begin{aligned}\frac{\mathrm{d}[e]_t}{\mathrm{d}t} &= \frac{\mathrm{d}[X]_t}{\mathrm{d}t} - \frac{\mathrm{d}[Y]_t}{\mathrm{d}t} \\ &= 2\left(k_2[B][Y]_t - k_1[A][X]_t\right) \\ &= -2k_1[A]\left([X]_t - \frac{k_2[B]}{k_1[A]}[Y]_t\right) \end{aligned} \tag{10}$$

If $k_1[A] = k_2[B]$ is satisfied, we can obtain

$$\frac{k_2[B]_0}{k_1[A]_0} = 1 \tag{11}$$

and Eq. (11) can be simplified to

$$\frac{d[e]_t}{dt} = -2k_1[A]\left([X]_t - [Y]_t\right) = -2k_1[A][e]_t \tag{12}$$

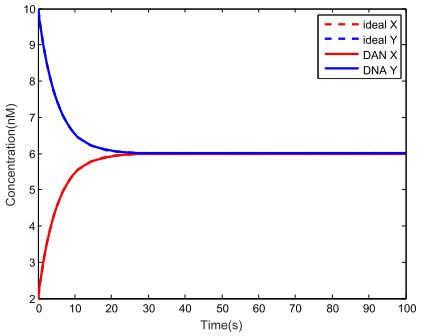

FIGURE 3. Synchronization for X and Y where $[X]_0 = 2$nM, $[Y]_0 = 10$nM; $[A]_0 = 10^3$nM, $[B]_0 = 10^3$nM; $k_1 = 10^{-5}$/nM/s, $k_2 = 10^{-5}$/nM/s.

Thus, from the Lyapunov theorem, complete synchronization of two different chemical species with different initial concentrations is realized.

When (1) reaches dynamic equilibrium,

$$[X]_\infty = [Y]_\infty = \frac{[X]_0 + [Y]_0}{2}, \tag{13}$$

since $[X]_t - [X]_0 = [Y]_0 - [Y]_t$, and $2k_1[A]$ is crucial to the synchronization speed.

C. INDIRECT SYNCHRONIZATION OF TWO DIFFERENT CHEMICAL SPECIES

If chemical specie X cannot react with A to produce Y reversibly, we can realize synchronization through the following CRNs

$$X + A_1 \underset{k2}{\overset{k_1}{\rightleftarrows}} W_1 + B_1 \tag{14}$$

$$Y + A_2 \underset{k4}{\overset{k_3}{\rightleftarrows}} W_2 + B_2 \tag{15}$$

so that

$$W_1 + A_3 \underset{k6}{\overset{k_5}{\rightleftarrows}} W_2 + B_3 \tag{16}$$

where $[e]_t = [X]_t - [Y]_t$.

Definition 3: If Eq. (17) is satisfied, complete synchronization between X and Y can be realized

$$\begin{cases} k_2[B_1]_0 = k_1[A_1]_0 \\ k_4[B_2]_0 = k_3[A_2]_0 \\ k_6[B_3]_0 = k_5[A_3]_0 \end{cases} \tag{17}$$

where

$$\begin{cases} C_m = [A_1]_0 = [B_1]_0 \gg [X]_0, [W_1]_0 \\ C_m = [A_2]_0 = [B_2]_0 \gg [Y]_0, [W_2]_0 \\ C_m = [A_3]_0 = [B_3]_0 \gg [W_1]_0, [W_2]_0 \end{cases} \tag{18}$$

The proof is similar to proof 2. Based on (14) and (15), X and W_1 are synchronized, Y and W_2 are synchronized, it is obvious that the synchronization between X and Y can be realized, because W_1 and W_2 are also synchronized according to (16).

D. SYNCHRONIZATION OF MULTIPLE DIFFERENT CHEMICAL SPECIES

We synchronize multiple CRNs as follows,

$$X + A_1 \underset{k2}{\overset{k_1}{\rightleftarrows}} Y_1 + B_1 \tag{19}$$

$$X + A_2 \underset{k4}{\overset{k_3}{\rightleftarrows}} Y_2 + B_2 \tag{20}$$

$$\vdots$$

$$X + A_n \underset{k2n}{\overset{k_{2n-1}}{\rightleftarrows}} Y_n + B_n, n \geq 1 \tag{21}$$

Definition 4: The synchronization between $\mathbf{X}$ and $\mathbf{Y_i(i = 1, \cdots, n)}$ can be obtained, if exist

$$\begin{cases} k_2 [B_1]_0 = k_1 [A_1]_0 \\ k_4 [B_2]_0 = k_3 [A_2]_0 \\ \vdots \\ k_{2n} [B_n]_0 = k_{2n-1} [A_n]_0 \end{cases} \tag{22}$$

where

$$\begin{cases} C_m = [A_1]_0 = [B_1]_0 \gg [X]_0, [Y_1]_0 \\ C_m = [A_2]_0 = [B_2]_0 \gg [X]_0, [Y_2]_0 \\ \vdots \\ C_m = [A_n]_0 = [B_n]_0 \gg [X]_0, [Y_n]_0 \end{cases} \tag{23}$$

The proof is similar to proof 2.

E. PROJECTIVE SYNCHRONIZATION

For projective synchronization, error between two different chemical species is defined as

$$[e]_t = n \times [X]_t - [Y]_t, \tag{24}$$

Definition 5: If $k_1 = nk_2$, exist $[e]_\infty = 0$, where $n \in R$ is scaling factor.

Proof 3:

$$\begin{aligned} \frac{\mathrm{d}[e]_t}{\mathrm{d}t} &= \frac{\mathrm{d}(n\,[X]_t)}{\mathrm{d}t} - \frac{\mathrm{d}[Y]_t}{\mathrm{d}t} \\ &= 2\,(k_2[B][Y]_t - k_1[A][X]_t) \\ &= 2k_2([B]\,[Y]_t - n[A][X]_t) \end{aligned} \tag{25}$$

Since$[A] = [B] = C_m$, (25) can be simplified to

$$\begin{aligned} \frac{\mathrm{d}[e]_t}{\mathrm{d}t} &= \frac{\mathrm{d}(n\,[X]_t)}{\mathrm{d}t} - \frac{\mathrm{d}[Y]_t}{\mathrm{d}t} \\ &= -2k_2[A](n[X]_t - [Y]_t) \\ &= -2k_2[A][e]_t. \end{aligned} \tag{26}$$

When (1) reaches dynamic equilibrium, since $[X]_t - [X]_0 = [Y]_0 - [Y]_t$ and $[Y]_\infty = [X]_\infty$, exist

$$\begin{cases} [X]_\infty = \dfrac{[X]_0 + [Y]_0}{n+1} \\ [Y]_\infty = \dfrac{n([X]_0 + [Y]_0)}{n+1}. \end{cases} \tag{27}$$

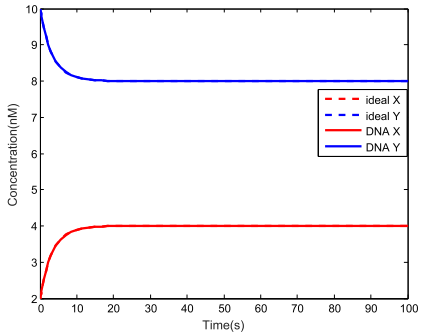

FIGURE 4. Projective synchronization for X and Y where $[X]_0 = 2$nM, $[Y]_0 = 10$nM;$[A]_0 = 10^4$nM, $[B]_0 = 10^4$nM; $k_1 = 10^{-5}$/nM/s, $k_2 = 10^{-5}$/nM/s, $n = 2$.

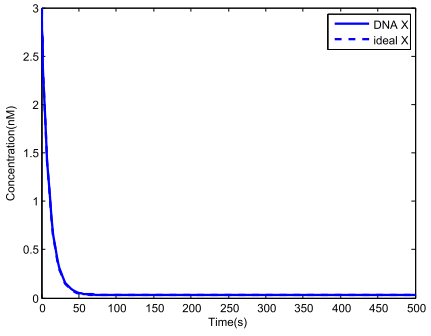

FIGURE 5. Degradation of X where $[X]_0 = 3$nM, $[Y]_0 = 10$nM; $[A]_0 = 10^2$nM, $[B]_0 = 10^2$nM;$k_1 = 10^{-5}$/nM/s, $k_2 = 10^{-3}$/nM/s.

As Fig. 4 shown, $[Y]_\infty = 2[X]_\infty$, because $n = 2$. Under the premise of projective synchronization of two different chemical species, the concentration of X will approach zero, as shown in Fig. 5, when $[Y]_0 \ll [X]_0$, $n \gg 1$. Thus, we realize degradation of X.

III. CRN MODULES

Approximation of ideal formal CRNs (30) can be realized by Visual DSD software [16]. Figure 6(a) shows the DSD implementation of catalysis reaction module 1. The auxiliary specie $A_i^{\pm}$ is displaced by single strand (ss) DNA $X_1^{\pm}$ at rate q_i, producing the intermediate complex $L_i^{\pm}$ and ss DNA $H_i^{\pm}$, which reacts with auxiliary specie $C_i^{\pm}$ to release two ss DNA $X_1^{\pm}$. Figure 6(b) shows that the catalysis processes of $X_1^{\pm}$ in DNA CRNs coincide with those of $X_1^{\pm}$ in ideal formal CRNs, which means that ideal formal CRNs (30) are suitable as corresponding DNA CRNs.

Fig. 7(a) shows the DSD implementation of catalysis reaction module 2. The reaction is initiated when ss DNA $X_1^{\pm}$ displaces auxiliary species $B_i^{\pm}$ reversibly, producing complex DNA strand $T_i^{\pm}$ and releasing ssDNA strand $F_i^{\pm}$ at rate q_m; $F_i^{\pm}$ reacts with complex $G_i^{\pm}$ releasing two ss DNA $X_2^{\pm}$. Fig. 7(b) shows that the catalysis processes of $X_1^{\pm}$ and $X_2^{\pm}$ in DNA CRNs coincide with in ideal formal CRNs, which means that ideal formal CRNs (34) is equivalent to corresponding DNA CRNs.

Fig. 8(a) shows the degradation reaction module implemented by DSD, $X_2^{\pm}$ is reversibly consumed by complex

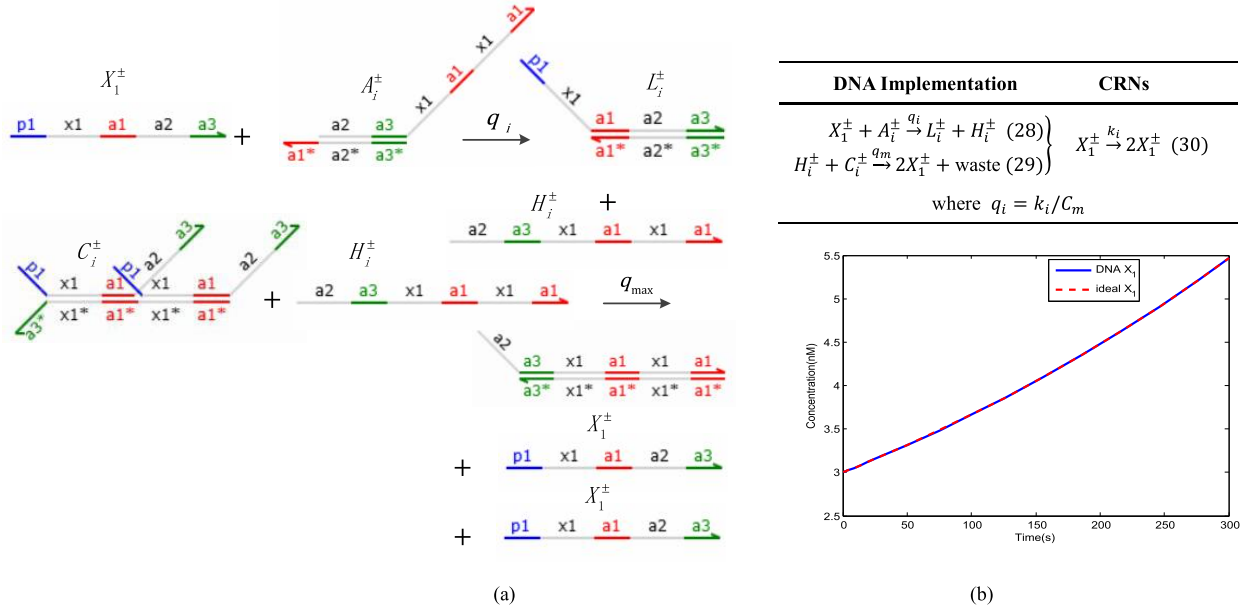

FIGURE 6. Catalysis reaction module 1: $X_1^{\pm} \rightarrow 2X_1^{\pm}$ (a) DNA reactions; (b) concentration evolution of $X_1^{\pm}$ in DNA CRNs and ideal formal CRNs respectively, where $C_m = 2 \times 10^4$nM and $[X_1^{\pm}]_0 = 3$nM; $q_i = 10^{-7}$/nM/s and $q_m = 10^{-3}$/nM/s. where q_m represents a maximum strand displacement rate constant under the assumption of equal binding strength for all full toeholds; C_{max} is the initial concentration of auxiliary complex strands $A_i^{\pm}$ and $C_i^{\pm}$; q_i and k_i are satisfied $q_i \leq q_m$, $k_i \leq q_m C_m$. The DNA reactions of Catalysis reaction module 1are adapted from [14].

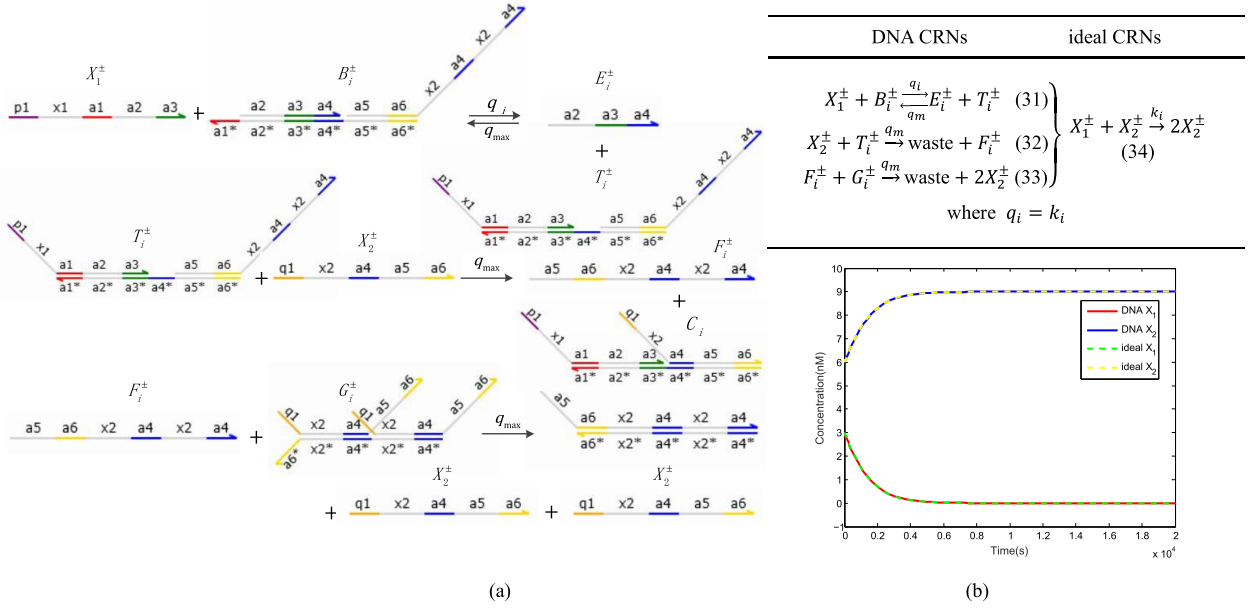

FIGURE 7. Catalysis reaction module 2: $X_1^{\pm} + X_2^{\pm} \xrightarrow{k_i} 2X_2^{\pm}$ (a) DNA reactions; (b) concentration evolutions of $X_1^{\pm}$ and $X_2^{\pm}$ in DNA CRNs and ideal formal CRNs respectively, where $C_m = 2 \times 10^4$nM, $[X_1^{\pm}]_0 = 3$nM, and $[X_2^{\pm}]_0 = 6$nM; $q_i = 10^{-4}$/nM/s and $q_m = 10^{-2}$/nM/s, C_{max} is the initial concentration of auxiliary complex strands $B_i^{\pm}$, $E_i^{\pm}$ and $G_i^{\pm}$. The DNA reactions of Catalysis reaction module 1are adapted from [14].

$M_i^{\pm}$ to produce inert waste. Fig. 8(b) shows that degradation processes of $X_2^{\pm}$ in DNA CRNs do not coincide with those of $X_2^{\pm}$ in ideal formal CRNs, because the reversible reaction cannot completely consume $X_2^{\pm}$.

Fig. 9(a) shows the DSD implementation of the annihilation reaction module, ss DNA X_1^+ and X_1^- are reversibly consumed by auxiliary species Fa_i and Fb_i respectively, producing ss DNA Dt_i and complex Ms_i. Dt_i reacts with Ms_i producing inert waste. Fig. 9(b) shows that the annihilation processes of $X_1^{\pm}$ and $X_2^{\pm}$ in DNA CRNs coincide with in ideal CRNs, which means that ideal formal CRNs (40) are equivalent to corresponding DNA CRNs.

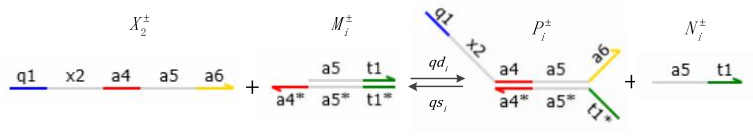

(a)

DNA CRNs	ideal CRNs
$X_2^{\pm} + M_i^{\pm} \underset{qs_i}{\overset{qd_i}{\rightleftarrows}} P_i^{\pm} + N_i^{\pm}$ (35)	$X_2^{\pm} \overset{k_i}{\to} \emptyset$, (36)
where $k_i = C_m q d_i$	

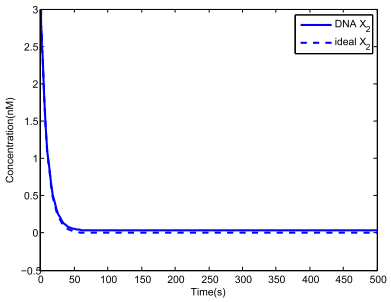

(b)

FIGURE 8. Degradation reaction module $X_2^{\pm} \to \emptyset$: DNA reactions are listed in (a); (b) represents evolution of degradation of X_2 in DNA CRNs and ideal formal CRNs respectively, where $C_m = 10^2$nM and $[X_2^{\pm}]_0 = 3$nM, $qd_i = 10^{-3}$/nM/s and $qs_i = 10^{-5}$/nM/s, C_{max} is the initial concentration of auxiliary complex strands M_i and N_i.

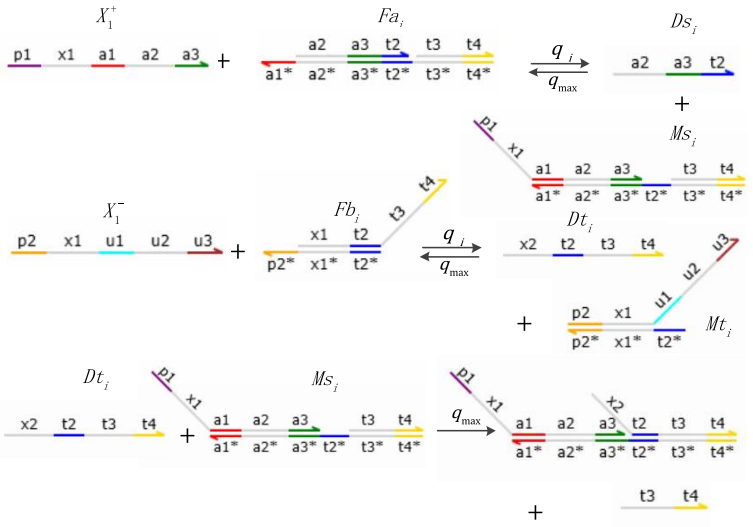

(a)

DNA Implementation	CRNs
$X_1^+ + Fa_i \underset{q_m}{\overset{q_i}{\rightleftarrows}} Ds_i + Ms_i$ (37) $X_1^- + Fb_i \underset{q_m}{\overset{q_i}{\rightleftarrows}} Dt_i + Mt_i$ (38) $Dt_i + Ms_i \overset{q_m}{\to}$ waste (39)	$X_1^+ + X_1^- \overset{k_i}{\to} \emptyset$ (40)
where $k_i = q_i^2/q_m$	

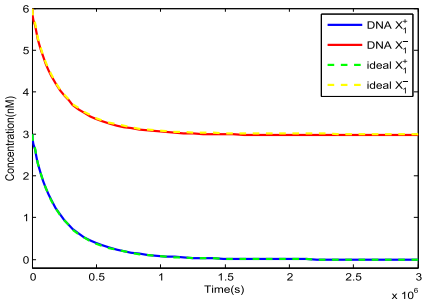

(b)

FIGURE 9. Annihilation reaction module $X_1^+ + X_1^- \to \emptyset$: DNA reactions are listed in (a); (b) represents evolution of annihilation of X_1^+ and X_1^- in DNA CRNs and ideal formal CRNs respectively, where $C_m = 2 \times 10^4$nM, $[X_1^+]_0 = 3$nM and $[X_1^-]_0 = 6$nM, $q_i = 10^{-4}$/nM/s and $q_m = 10^{-2}$/nM/s, C_{max} is the initial concentration of auxiliary complex strands Fa_i, Fb_i and Ms_i.

Fig. 10(a) shows the DNA reaction list for the synchronization or projective synchronization reaction module. Complex DNA strands $Dx_i^{\pm}$ and $Dy_i^{\pm}$ are displaced by $X_1^{\pm}$ and $Y_1^{\pm}$, respectively and reversibly, $Wx_i^{\pm}$ and $Wy_i^{\pm}$ are displaced by $Dz_i^{\pm}$ and $Jz_i^{\pm}$ respectively. Figs. 10(b) and (c) show that the synchronization and projective synchronization processes of $X_1^{\pm}$ and $Y_1^{\pm}$ in DNA CRNs are coincide with those of $X_1^{\pm}$ and $Y_1^{\pm}$ in ideal formal CRNs, which means that ideal CRNs (44) are suitable as corresponding DNA CRNs.

IV. RESULTS

A. LOTKA-VOLTERRA OSCILLATOR

The Lotka-Volterra oscillator is an ecological food chain oscillator, and a famous mathematical principle to describe predator-prey dynamics. The basic Lotka-Volterra oscillator [14] can be described as ideal formal CRNs

$$X_1 \xrightarrow{k_1} 2X_1 \tag{45a}$$
$$X_1 + X_2 \xrightarrow{k_2} 2X_2 \tag{45b}$$
$$X_2 \xrightarrow{k_3} \phi \tag{45c}$$

From (45a), the product of X_1 increases the product of X_2, and (45b) is catalyzed by X_2. Thus, increasing X_2 consumes more X_1, which slows (45b), and consequently decreases X_2. Therefore, concentrations of X_1 and X_2 fluctuate.

The CRNs (45) were converted to a DNA strand displacement system, but X_1 and X_2 are positive, because they represented the concentrations of X_1 and X_2, respectively, and the concentration is positive, as shown in Fig. 11(a). To extend the range of X_1 and X_2, the basic Lotka-Volterra oscillator

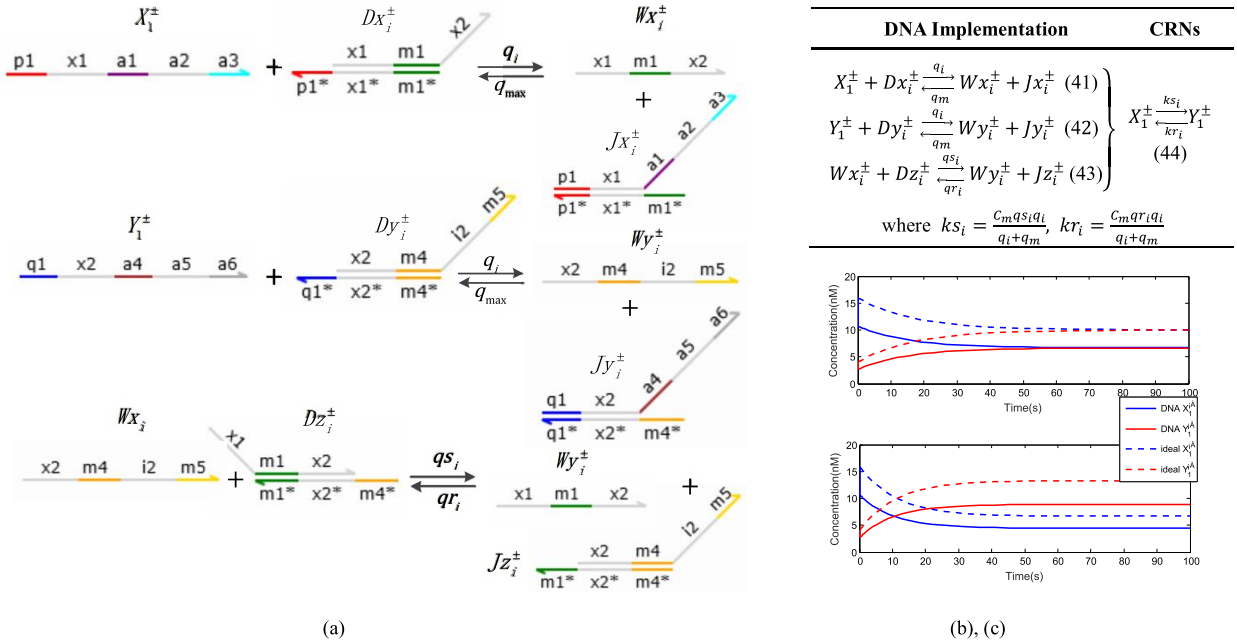

FIGURE 10. Synchronization or projective synchronization reaction module $X_1^{\pm}Y_1^{\pm}$: DNA reactions are listed in (a); (b) represents evolution of synchronization among $X_1^{\pm}$ and $Y_1^{\pm}$ in DNA CRNs and ideal formal CRNs respectively, where $C_m = 1 \times 10^4$nM, $[X_1]_0 = 16$nM and $[Y_1]_0 = 4$nM; $q_i = 10^{-3}$/nM/s, $qs_i = 10^{-5}$/nM/s, $qr_i = 10^{-5}$/nM/s and $q_m = 2 \times 10^{-3}$/nM/s. (c) represents evolution of projective synchronization among $X_1^{\pm}$ and $Y_1^{\pm}$ in DNA CRNs and idea CRNs respectively, where $C_m = 1 \times 10^4$nM, $[X_1]_0 = 16$nM and $[Y_1]_0 = 4$nM; $q_i = 10^{-3}$/nM/s, $qs_i = 2 \times 10^{-5}$/nM/s, $qr_i = 10^{-5}$/nM/s and $q_m = 2 \times 10^{-3}$/nM/s. C_{max} is the initial concentration of auxiliary complex strands $Dx_i^{\pm}$, $Dy_i^{\pm}$, $Dz_i^{\pm}$, $Jx_i^{\pm}$, $Jy_i^{\pm}$ and $Jz_i^{\pm}$.

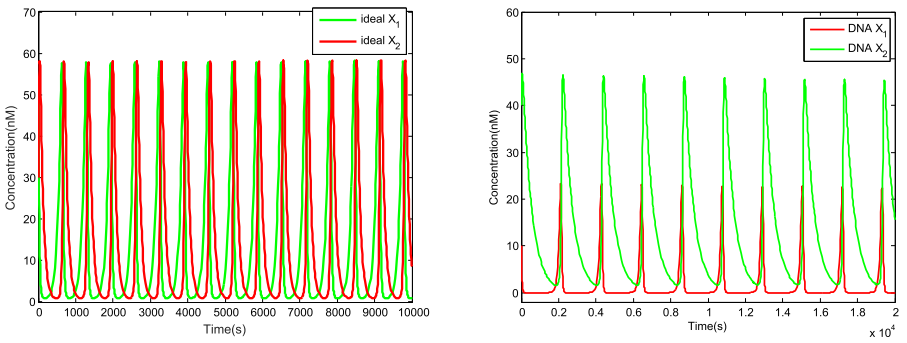

FIGURE 11. (a), (b): Evolution of concentrations of X_1 and X_2 for the basic Lotka-Volterra oscillator in ideal CRNs and DNA CRNs, where $[X_1]_0 = 10$nM and $[X_2]_0 = 40$nM; $k_1 = 1.334 \times 10^{-2}$/nM/$s$, $k_2 = 10^{-3}$/nM/s and $k_3 = 2 \times 10^{-3}$/nM/s. $C_m = 2 \times 10^4$nM; $q_1 = 10^{-4}$/nM/s and $q_m = 10^{-2}$/nM/s.

model (45) can be modified as ideal CRNs (46)

$$X_1^{\pm} \xrightarrow{k_1} 2X_1^{\pm} \tag{46a}$$

$$X_1^{\pm} + X_2^{\pm} \xrightarrow{k_2} 2X_2^{\pm} \tag{46b}$$

$$X_2^{\pm} \xrightarrow{k_3} \emptyset \tag{46c}$$

$$X_1^{+} + X_1^{-} \xrightarrow{k_4} \emptyset \tag{46d}$$

$$X_2^{+} + X_2^{-} \xrightarrow{k_4} \emptyset \tag{46e}$$

where the species $X_i^+ (i = 1, 2)$ and X_i^- are referred to represent the positive and negative component of value of X_i, with annihilation reaction (46d) and (46e), so that $X_i = X_i^+ - X_i^-$.

CRNs (46) can also be described by DNA reaction modules as follows:

$$X_1^{\pm} + A_1^{\pm} \xrightarrow{q_1} H_1^{\pm} + L_1^{\pm} \tag{47a}$$

$$H_1^{\pm} + C_1^{\pm} \xrightarrow{q_m} 2X_1^{\pm} + \text{waste} \tag{47b}$$

$$X_1^{\pm} + B_1^{\pm} \underset{qm}{\overset{q_2}{\rightleftarrows}} T_1^{\pm} + E_1^{\pm} \tag{48a}$$

$$X_2^{\pm} + T_1^{\pm} \xrightarrow{q_m} \text{waste} + F_1^{\pm} \tag{48b}$$
$$F_1^{\pm} + G_1^{\pm} \xrightarrow{q_m} \text{waste} + 2X_2^{\pm} \tag{48c}$$
$$X_2^{\pm} + M_1^{\pm} \underset{q4}{\overset{q_3}{\rightleftarrows}} P_1^{\pm} + N_1^{\pm} \tag{49}$$
$$X_1^{+} + Fa_1 \underset{qm}{\overset{q_5}{\rightleftarrows}} Ds_1 + Ms_1, \tag{50a}$$
$$X_1^{-} + Fa_2 \underset{qm}{\overset{q_5}{\rightleftarrows}} Ds_2 + Ms_2 \tag{50b}$$
$$Ds_1 + Ms_2 \xrightarrow{q_m} \text{waste} \tag{50c}$$
$$X_2^{+} + Fa_3 \underset{qm}{\overset{q_5}{\rightleftarrows}} Ds_3 + Ms_3 \tag{51a}$$
$$X_2^{-} + Fa_4 \underset{qm}{\overset{q_5}{\rightleftarrows}} Ds_4 + Ms_4, \tag{51b}$$
$$Ds_3 + Ms_4 \xrightarrow{q_m} \text{waste}. \tag{51c}$$

Fig. 11 shows the evolution of X and Y for the basic Lotka-Volterra oscillator in DNA and ideal formal CRNs.

B. SYNCHRONIZATION OF TWO PROPOSED LOTKA-VOLTERRA OSCILLATORS

Ideal formal CRNs (46) are assumed as the target system, and the response system is defined as

$$Y_1^{\pm} \xrightarrow{k_1} 2Y_1^{\pm} \tag{52a}$$
$$Y_1^{\pm} + Y_2^{\pm} \xrightarrow{k_2} 2Y_2^{\pm} \tag{52b}$$
$$Y_2^{\pm} \xrightarrow{k_3} \emptyset \tag{52c}$$
$$Y_1^{+} + Y_1^{-} \xrightarrow{k_4} \emptyset \tag{52d}$$
$$Y_2^{+} + Y_2^{-} \xrightarrow{k_4} \emptyset \tag{52e}$$

Then, we add the synchronization reaction module to the target and response systems as (53)

$$X_1^{\pm} \underset{k_s}{\overset{k_s}{\rightleftarrows}} Y_1^{\pm} \tag{53a}$$
$$X_2^{\pm} \underset{k_s}{\overset{k_s}{\rightleftarrows}} Y_2^{\pm} \tag{53b}$$

The dynamics of X_1^+ and X_1^- are then

$$\begin{cases} \dfrac{dX_1^+}{dt} = k_1 X_1^+ - k_2 X_1^+ X_2^+ - k_s\left(Y_1^+ - X_1^+\right) - k_4 X_1^+ X_1^- \\ \dfrac{dX_1^-}{dt} = k_1 X_1^- - k_2 X_1^- X_2^- - k_s\left(Y_1^- - X_1^-\right) - k_4 X_1^+ X_1^- \end{cases} \tag{54}$$

Therefor

$$\begin{aligned} \frac{dX_1}{dt} &= \frac{dX_1^+}{dt} - \frac{dX_1^-}{dt} \\ &= k_1 X_1^+ - k_2 X_1^+ X_2^+ + k_s\left(Y_1^+ - X_1^+\right) - k_4 X_1^+ X_1^- \\ &\quad - \left(k_1 X_1^- - k_2 X_1^- X_2^- + k_s\left(Y_1^- - X_1^-\right) - k_4 X_1^+ X_1^-\right) \\ &= k_1\left(X_1^+ - X_1^-\right) - k_2\left((X_1X_2)^+ - (X_1X_2)^-\right) \\ &\quad + k_s(Y_1^+ - Y_1^-) - k_s(X_1^+ - X_1^-) \end{aligned} \tag{55}$$

where $(X_1X_2)^+ = X_1^+X_2^+$ and $(X_1X_2)^- = X_1^-X_2^-$, and Eq. (55) can be further simplified as

$$\frac{dX_1}{dt} = k_1X_1 - k_2X_1X_2 + k_s(Y_1 - X_1) \tag{56}$$

Similarly dynamics of X_2, Y_1 and Y_2 can be obtained as

$$\frac{dX_2}{dt} = k_2X_1X_2 - k_3X_2 + k_s(Y_2 - X_2) \tag{57}$$
$$\frac{dY_1}{dt} = k_1Y_1 - k_2Y_1Y_2 + k_s(X_1 - Y_1) \tag{58}$$
$$\frac{dY_2}{dt} = k_2Y_1Y_2 - k_3Y_2 + k_s(X_2 - Y_2) \tag{59}$$

Define the error state as $e_i = Y_i - X_i$ $(i = 1, 2)$, and the dynamics of error can be described as

$$\begin{cases} \dfrac{de_1}{dt} = (k_1 - 2k_s)e_1 + \Phi_1(X_1) - \Phi_2(Y_1) \\ \dfrac{de_2}{dt} = -(k_3 + 2k_s)e_2 + \Psi_2(Y_2) - \Psi_1(X_2) \end{cases} \tag{60}$$

where $\Phi_1(X_1) = k_2X_1X_2$, $\Phi_2(Y_1) = k_2Y_1Y_2$, $\Psi_1(X_2) = k_2X_1X_2$, $\Psi_2(Y_2) = k_2Y_1Y_2$.

Definition 6: The complete synchronization between the CRNs (46) and the CRNs (52) can be realized by adding synchronization reaction module, if the inequalities $\varepsilon_1 + k_1 - 2k_s < 0$ and $\varepsilon_2 - k_3 - 2ks < 0$ are satisfied.

Proof 4: Considering the following Lyapunov function:

$$V(t) = \sum_{i=1}^{2} \frac{1}{2} e_i^{\mathrm{T}}(t)\, e_i(t) \tag{61}$$

The time derivative of $V(t)$ is

$$\begin{aligned} \frac{dV(t)}{dt} &= \sum_{i=1}^{2} \frac{1}{2} e_i^{\mathrm{T}}(t)\dot{e}_i(t) \\ &= e_1\left((k_1 - 2k_s)e_1 + \Phi_1(X_1) - \Phi_2(Y_1)\right) \\ &\quad + e_2\left(-(k_3 + 2k_s)e_2 + \Psi_2(Y_2) - \Psi_1(X_2)\right) \end{aligned} \tag{62}$$

For the real number $\varepsilon_1, \varepsilon_2 > 0$, the following relationships are set up through utilizing of Lipschitz condition:

$$\|\Phi_1(X_1) - \Phi_2(Y_1)\| \le \varepsilon_1 \|X_1 - Y_1\| \tag{63}$$
$$\|\Psi_1(X_2) - \Psi_2(Y_2)\| \le \varepsilon_2 \|X_2 - Y_2\| \tag{64}$$

and Eq. (61) can be simplified as follow:

$$\frac{dV(t)}{dt} \le (\varepsilon_1 + k_1 - 2k_s)\, e_1^2 + (\varepsilon_2 - k_3 - 2k_s)\, e_2^2 \tag{65}$$

If the inequalities $\varepsilon_1 + k_1 - 2k_s < 0$ and $\varepsilon_2 - k_3 - 2k_s < 0$ are hold, it is easy to obtain $dV(t)/dt < 0$. Based on Lyapunov stability, the errors of two CRNs systems are asymptotically stable, and the Theorem 5 is proved.

The ideal formal CRNs (52) and reaction (53) can be approximated as DNA reaction modules

$$Y_1^{\pm} + A_2^{\pm} \xrightarrow{q_1} H_2^{\pm} + L_2^{\pm} \tag{66a}$$
$$H_2^{\pm} + C_2^{\pm} \xrightarrow{q_m} 2Y_1^{\pm} + \text{waste} \tag{66b}$$
$$Y_1^{\pm} + B_2^{\pm} \underset{qm}{\overset{q_2}{\rightleftarrows}} T_2^{\pm} + E_2^{\pm} \tag{67a}$$

$$Y_2^{\pm} + T_2^{\pm} \xrightarrow{q_m} \text{waste} + F_2^{\pm} \tag{67b}$$
$$F_2^{\pm} + G_2^{\pm} \xrightarrow{q_m} \text{waste} + 2Y_2^{\pm} \tag{67c}$$
$$Y_2^{\pm} + M_2^{\pm} \underset{q4}{\overset{q3}{\rightleftarrows}} P_2^{\pm} + N_2^{\pm} \tag{68}$$
$$Y_1^{+} + Fa_5 \underset{qm}{\overset{q5}{\rightleftarrows}} Ds_5 + Ms_5 \tag{69a}$$
$$Y_1^{-} + Fa_6 \underset{qm}{\overset{q5}{\rightleftarrows}} Ds_6 + Ms_6 \tag{69b}$$
$$Ds_5 + Ms_6 \xrightarrow{q_m} \text{waste} \tag{69c}$$
$$Y_2^{+} + Fa_7 \underset{qm}{\overset{q5}{\rightleftarrows}} Ds_7 + Ms_7 \tag{70a}$$
$$Y_2^{-} + Fa_8 \underset{qm}{\overset{q5}{\rightleftarrows}} Ds_8 + Ms_8 \tag{70b}$$
$$Ds_7 + Ms_8 \xrightarrow{q_m} \text{waste} \tag{70c}$$
$$\begin{cases} X_1^{\pm} + D_1^{\pm} \underset{qm}{\overset{q6}{\rightleftarrows}} W_1^{\pm} + J_1^{\pm} \\ Y_1^{\pm} + D_2^{\pm} \underset{qm}{\overset{q6}{\rightleftarrows}} W_2^{\pm} + J_2^{\pm} \\ W_1^{\pm} + D_3^{\pm} \underset{q7}{\overset{q7}{\rightleftarrows}} W_2^{\pm} + J_3^{\pm} \end{cases} \tag{71a}$$
$$\begin{cases} X_2^{\pm} + D_4^{\pm} \underset{qm}{\overset{q6}{\rightleftarrows}} W_3^{\pm} + J_4^{\pm} \\ Y_2^{\pm} + D_5^{\pm} \underset{qm}{\overset{q6}{\rightleftarrows}} W_4^{\pm} + J_5^{\pm} \\ W_3^{\pm} + D_6^{\pm} \underset{q7}{\overset{q7}{\rightleftarrows}} W_4^{\pm} + J_6^{\pm} \end{cases} \tag{71b}$$

Visual DSD software can realize approximations of the ideal formal CRNs (46) and (52). The catalysis reactions (47) and (66) are realized by catalysis module 1 as shown in Fig. 6. The DSD implementation of the catalysis reactions (48) and (67) are shown in Fig. 7. The DSD implementation of reactions (47) and (66) can be realized by degradation reaction module, as shown in Fig. 8. Reactions (50), (51), (69) and (70) are annihilation reactions, which can be realized by the annihilation reaction module. Finally, the DSD implementation of reaction (71) can be obtained by the synchronization or projective synchronization reaction modules.

C. PROJECTIVE SYNCHRONIZATION OF TWO PROPOSED LOTKA-VOLTERRA OSCILLATORS

To realize projective synchronization of two proposed Lotka-Volterra oscillators, we add the projective synchronization reaction module to the target and response systems as:

$$X_1^{\pm} \underset{k_r}{\overset{k_s}{\rightleftarrows}} Y_1^{\pm} \tag{72a}$$
$$X_2^{\pm} \underset{k_r}{\overset{k_s}{\rightleftarrows}} Y_2^{\pm} \tag{72b}$$

And dynamics of X_2, Y_1 and Y_2 can be written as

$$\begin{cases} \dfrac{\mathrm{d}X_1}{\mathrm{d}t} = k_1 X_1 - k_2 X_1 X_2 + k_s Y_1 - k_r X_1 \\ \dfrac{\mathrm{d}X_2}{\mathrm{d}t} = k_2 X_1 X_2 - k_3 X_2 + k_s Y_2 - k_r X_2 \end{cases} \tag{73}$$

$$\begin{cases} \dfrac{\mathrm{d}Y_1}{\mathrm{d}t} = k_1 Y_1 - k_2 Y_1 Y_2 + k_s X_1 - k_r Y_1 \\ \dfrac{\mathrm{d}Y_2}{\mathrm{d}t} = k_2 Y_1 Y_2 - k_3 Y_2 + k_s X_2 - k_r Y_2 \end{cases} \tag{74}$$

In order to show the projective synchronization of two CRNs systems, the error between state variables of system is defined as $e_i^{'} = Y_i - \alpha X_i$ $(i = 1, 2)$, and the dynamics of error can be described as

$$\begin{cases} \dfrac{\mathrm{d}e_1^{'}}{\mathrm{d}t} = (k_1 - 2k_r)e_1 + \Lambda_1(X_1) - \Lambda_2(Y_1) \\ \dfrac{\mathrm{d}e_2^{'}}{\mathrm{d}t} = -(k_3 + 2k_r)e_2 + K_2(Y_2) - K_1(X_2) \end{cases} \tag{75}$$

where $\Lambda_1(X_1) = k_2 X_1 X_2 + k_1(k_s/k_r - 1)X_1$, $\Lambda_2(Y_1) = k_2 Y_1 Y_2$, $K_1(X_2) = k_2 X_1 X_2 - k_3(k_s/k_r - 1)X_2$, $K_2(Y_2) = k_2 Y_1 Y_2$, $\alpha = k_s/k_r$.

Definition 7: The projective synchronization between the CRNs (46) and the CRNs (52) can be realized by adding projective synchronization reaction module, if the inequalities $\xi_1 + k_1 - 2k_r < 0$ and $\xi_2 - k_3 - 2k_r < 0$ are satisfied.

Proof 5: The time derivative of $V^{'}(t)$ is

$$\begin{aligned} \frac{\mathrm{d}V^{'}(t)}{\mathrm{d}t} &= \sum_{i=1}^{2} \frac{1}{2} e_i^{'\mathrm{T}}(t)\dot{e}_i^{'}(t) \\ &= e_1^{'}\left((k_1 - 2k_r)e_1^{'} + \Lambda_1(X_1) - \Lambda_2(Y_1)\right) \\ &\quad + e_2^{'}\left(-(k_3 + 2k_r + K_2(Y_2) - K_1(X_2)\right) \end{aligned} \tag{76}$$

For the real number $\xi_1, \xi_2 > 0$, the following relationships are set up through utilizing of Lipschitz condition:

$$\|\Lambda_1(X_1) - \Lambda_2(Y_1)\| \le \xi_1 \|X_1 - Y_1\| \tag{77}$$
$$\|K_1(X_2) - K_2(Y_2)\| \le \xi_2 \|X_2 - Y_2\| \tag{78}$$

and Eq. (76) can be simplified as follow:

$$\frac{\mathrm{d}V^{'}(t)}{\mathrm{d}t} \le (\xi_1 + k_1 - 2k_r)\, e_1^2 + \left(\xi_2 - k_3 - 2k_r\right) e_2^2 \tag{79}$$

If the inequalities $\xi_1 + k_1 - 2k_s < 0$ and $\xi_2 - k_3 - 2k_s < 0$ are hold, it is easy to obtain $\mathrm{d}V^{'}(t)/dt < 0$. Based on Lyapunov stability, projective synchronization of the CRNs (46) and the CRNs (52) can be achieved.

The ideal formal reaction (72) can be approximated as

$$\begin{cases} X_1^{\pm} + D_7^{\pm} \underset{qm}{\overset{q6}{\rightleftarrows}} W_6^{\pm} + J_7^{\pm} \\ Y_1^{\pm} + D_8^{\pm} \underset{qm}{\overset{q6}{\rightleftarrows}} W_7^{\pm} + J_8^{\pm} \\ W_6^{\pm} + D_9^{\pm} \underset{q8}{\overset{q7}{\rightleftarrows}} W_7^{\pm} + J_9^{\pm} \end{cases} \tag{80}$$

and

$$\begin{cases} X_2^{\pm} + D_{10}^{\pm} \underset{qm}{\overset{q6}{\rightleftarrows}} W_8^{\pm} + J_{10}^{\pm} \\ Y_2^{\pm} + D_{11}^{\pm} \underset{qm}{\overset{q6}{\rightleftarrows}} W_9^{\pm} + J_{11}^{\pm} \\ W_8^{\pm} + D_{12}^{\pm} \underset{q8}{\overset{q7}{\rightleftarrows}} W_9^{\pm} + J_{12}^{\pm} \end{cases} \tag{81}$$

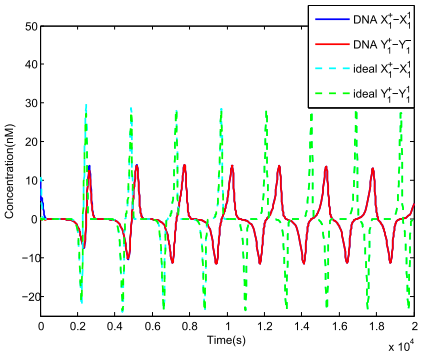

FIGURE 12. Concentration evolution of $X_1^+ - X_1^-$ and $Y_1^+ - Y_1^-$ for the proposed Lotka-Volterra oscillator.

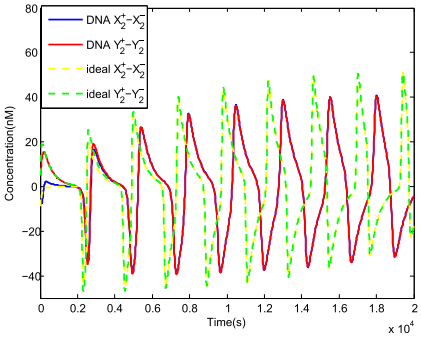

FIGURE 13. Concentration evolution of $X_2^+ - X_2^-$ and $Y_2^+ - Y_2^-$ for the proposed Lotka-Volterra oscillator.

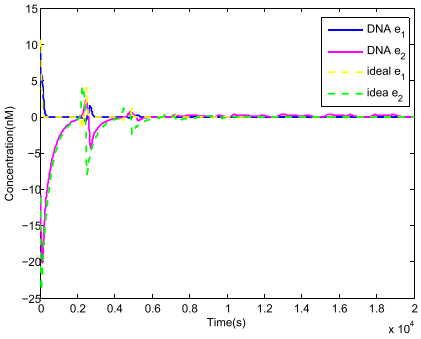

FIGURE 14. Error evolution for the proposed Lotka-Volterra oscillator.

V. SIMULATION RESULTS

A. SYNCHRONIZATION OF PROPOSED LOTKA-VOLTERRA OSCILLATOR

Table 1 shows the Lotka-Volterra oscillator parameters, where $[X_1^+]_0$, $[X_1^-]_0$, $[X_2^+]_0$, $[Y_1^+]_0$, $[Y_1^-]_0$, $[Y_2^=]_0$, and $[Y_2^-]_0$ represent the initial value of species X_1^+, X_1^-, X_2^+, X_2^-, Y_1^+, Y_1^-, Y_2^+ and Y_2^- respectively, where $[X_1^+]_0 = 30$nM, $[X_1^-]_0 = 20$nM, $[X_2^+]_0 = 4$nM, $[X_2^-]_0 = 10$nM, $[Y_1^+]_0 = 30$nM, $[Y_1^-]_0 = 30$nM, $[Y_2^+]_0 = 20$nM, and $[Y_2^-]_0 = 15$nM. Initial concentrations of the auxiliary species $A_1^\pm$, $C_1^\pm$, $B_1^\pm$, $E_1^\pm$, $G_1^\pm$, $M_1^\pm$, $N_1^\pm$, Fa_1, Fa_2, Ms_1, Ds_2, Fa_3, Ms_3, Fa_4, Ds_4, $A_2^\pm$, $C_2^\pm$, $B_2^\pm$, $E_2^\pm$, $G_2^\pm$, $M_2^\pm$, $N_2^\pm$, Fa_5, Fa_6, Ds_6, Ms_5, Fa_7, Ms_7, Fa_8, Ds_8, $D_i^\pm$, and $J_i^\pm$ $(i = 1, \cdots, 6)$ were set to C_m, and initial concentration of the auxiliary species $P_1^\pm$ and $P_2^\pm$ were fixed as 0.1 nM.

TABLE 1. Proposed Lotka-Volterra oscillator parameter values

	Value		Value		Value
k_1	$4/300$/s	q_1	$k_1 C_m^{-1}$	C_m	2×10^{-5}M
k_2	10^6/M/s	q_2	k_2	q_m	10^6/M/s
k_3	$2/1000$/s	q_3	$k_3 C_m^{-1}$	q_4	10^{-2}/M/s
k_4	100/M/s	q_5	$\sqrt{k_4 q_m}$	q_6	10^4/M/s
ks	2×10^6/M/s	q_7	$\frac{ks(q_6+q_m)}{C_m q_6}$		

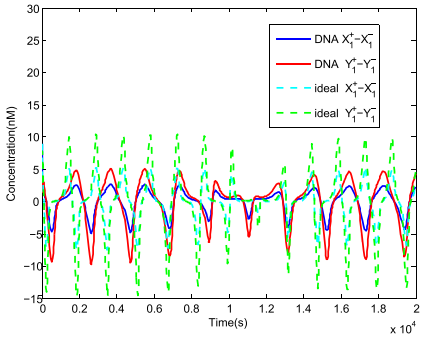

FIGURE 15. Concentration evolution of $X_1^+ - X_1^-$ and $Y_1^+ - Y_1^-$ for the proposed Lotka-Volterra oscillator added synchronization reaction.

Fig. 12 shows the concentration evolution of $X_1^+ - X_1^-$ and $Y_1^+ - Y_1^-$, and Fig. 13 shows the concentration evolution of $X_2^+ - X_2^-$, $Y_2^+ - Y_2^-$ for the proposed Lotka-Volterra oscillator. Fig. 14 shows the error evolution for

$$\begin{cases} e_1 = [X_1^+]_t - [X_1^-]_t - \left([Y_1^+]_t - [Y_1^-]_t\right) \\ e_2 = [X_2^+]_t - [X_2^-]_t - \left([Y_2^+]_t - [Y_2^-]_t\right) \end{cases} \tag{82}$$

From Figure 12–14, concentration evolution of $X_1^+ - X_1^-$ (or $X_2^+ - X_2^-$), $Y_1^+ - Y_1^-$ (or $Y_2^+ - Y_2^-$), and errors of the proposed Lotka-Volterra oscillator in DNA CRNs is similar to those for ideal formal CRNs, which demonstrates that the synchronization strategy in ideal formal CRNs is equivalent to corresponding DNA CRNs.

B. PROJECTIVE SYNCHRONIZATION OF PROPOSED LOTKA-VOLTERRA OSCILLATOR

Table 2 shows the projective synchronization reaction module parameters, where $[X_1^+]_0 = 10$nM, $[X_1^-]_0 = 1$nM, $[X_2^+]_0 = 3$nM, $[X_2^-]_0 = 2$nM, $[Y_1^+]_0 = 6$nM, $[Y_1^-]_0 = 20$nM, $[Y_2^+]_0 = 3$nM, and $[Y_2^-]_0 = 5$nM. Initial concentrations of the auxiliary species $D_i^\pm$ and $J_i^\pm$ $(i = 7, \cdots, 12)$ were set to C_m.

Fig 15 shows the concentration evolution of $X_1^+ - X_1^-$, $Y_1^+ - Y_1^-$, and Fig. 16 of $X_2^+ - X_2^-$, $Y_2^+ - Y_2^-$ for the proposed Lotka-Volterra oscillator. Figure 17 shows the error evolution for

$$\begin{cases} e_1' = 2\left([X_1^+]_t - [X_1^-]_t\right) - \left([Y_1^+]_t - [Y_1^-]_t\right) \\ e_2' = 2\left([X_2^+]_t - [X_2^-]_t\right) - \left([Y_2^+]_t - [Y_2^-]_t\right) \end{cases} \tag{83}$$

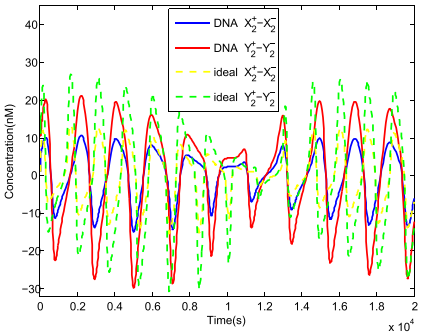

FIGURE 16. Concentration evolution of $X_2^+ - X_2^-$ and $Y_2^+ - Y_2^-$ for the proposed Lotka-Volterra oscillator added synchronization reaction.

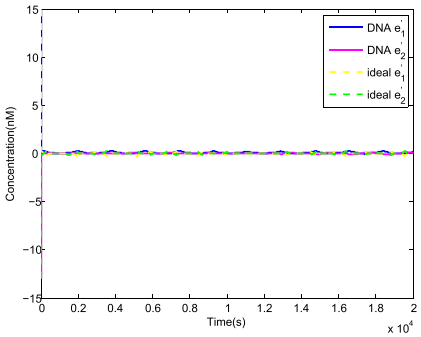

FIGURE 17. Error evolution for the proposed Lotka-Volterra oscillator.

TABLE 2. Proposed Lotka-Volterra oscillator parameter values

	Value		Value		Value
k_1	$4/300$/s	q_1	$k_1 C_m^{-1}$	C_m	2×10^{-5}M
k_2	10^6/M/s	q_2	k_2	q_m	10^6/M/s
k_3	$2/1000$/s	q_3	$k_3 C_m^{-1}$	q_4	10^{-2}/M/s
k_4	100/M/s	q_5	$\sqrt{k_4 q_m}$	q_6	10^4/M/s
ks	4×10^8/M/s	q_7	$\frac{ks(q_6+q_m)}{C_m q_6}$		
kr	2×10^8/M/s	q_8	$\frac{kr(q_6+q_m)}{C_m q_6}$		

From Figs. 15–17, concentration evolution of $X_1^+ - X_1^-$ (or $X_2^+ - X_2^-$), $Y_1^+ - Y_1^-$ (or $Y_2^+ - Y_2^-$), when we added synchronization reaction to CRNs, and errors of the proposed Lotka-Volterra oscillator in DNA CRNs are similar to those for ideal formal CRNs, which means that projective synchronization strategy in ideal formal CRNs is equivalent to corresponding DNA CRNs.

VI. CONCLUSIONS

Reversible chemical reactions in error degradation of two chemical species, and synchronization or projective synchronization of two chemical species are investigated in this article.

We realized degradation reactions by reversible chemical reactions, and proposed two types of catalysis, degradation, and annihilation reactions; as well as synchronization and projective synchronization reaction modules implemented by DNA CRNs.

Relationships between ideal formal CRNs and DNA CRNs for these modules were analyzed by using a proposed Lotka-Volterra oscillator as example to validate the effectiveness of the proposed strategies for synchronization or projective synchronization in ideal formal CRNs and DNA CRNs.

ACKNOWLEDGMENT

The authors thank LetPub (www.letpub.com) for linguistic assistance during the preparation of this manuscript.

REFERENCES

[1] W. Li, F. Zhang, H. Yan, and Y. Liu, "DNA based arithmetic function: A half adder based on DNA strand displacement," *Nanoscale*, vol. 8, no. 6, pp. 3775–3784, Feb. 2016.

[2] J. W. Sun, X. Li, G. Z. Cui, and Y. F. Wang, "One-bit half adder-half subtractor logical operation based on the DNA strand displacement," *J. Nanoelectron. Optoelectron.*, vol. 12, no. 4, pp. 375–380, Apr. 2017.

[3] M. R. Lakin and D. Stefanovic, "Supervised learning in adaptive DNA strand displacement networks," *ACS Synth. Biol.*, vol. 5, no. 8, pp. 885–897, Aug. 2016.

[4] L. Qian, E. Winfree, and J. Bruck, "Neural network computation with DNA strand displacement cascades," *Nature*, vol. 475, no. 7356, pp. 368–372, Jul. 2011.

[5] L. Qian and E. Winfree, "Scaling up digital circuit computation with DNA strand displacement cascades," *Science*, vol. 332, no. 6034, pp. 1196–1201, Jun. 2011.

[6] X. T. Ji, H. Y. Lv, M. H. Ma, B. L. Lv, and C. F. Ding, "An optical DNA logic gate based on strand displacement and magnetic separation, with response to multiple microRNAs in cancer cell lysates," *Microchimica ACTA*, vol. 184, no. 8, pp. 2505–2513, Aug. 2017.

[7] J. Fern and R. Schulman, "Design and characterization of DNA strand-displacement circuits in serum-supplemented cell medium," *ACS Synth. Biol.*, vol. 6, no. 9, pp. 1774–1783, Sep. 2017.

[8] T. Song, S. Garg, R. Mokhtar, H. Bui, and J. Reif, "Analog computation by DNA strand displacement circuits," *Acs Synth. Biol.*, vol. 5, no. 8, pp. 898–912, Aug. 2016.

[9] C. Y. Zou, X. P. Wei, Q. Zhang, C. J. Liu, C. J. Zhou, and Y. Liu, "Four-analog computation based on DNA strand displacement," *ACS Omega*, vol. 2, no. 8, pp. 4143–4160, Aug. 2017.

[10] J. Fern, D. Scalise, A. Cangialosi, D. Howie, L. Potters, and R. Schulman, "DNA strand-displacement timer circuits," *ACS Synth. Biol.*, vol. 6, no. 2, pp. 190–193, Feb. 2017.

[11] B. Wang, X. J. Wang, B. Wei, F. J. Huang, D. B. Yao, and H. J. Liang, "DNA photonic nanowires with tunable FRET signals on the basis of toehold-mediated DNA strand displacement reactions," *Nanoscale*, vol. 9, no. 9, pp. 2981–2985, Mar. 2017.

[12] K. Oishi and E. Klavins, "Biomolecular implementation of linear I/O systems," *IET Syst. Biol.*, vol. 5, no. 4, pp. 252–260, Jul. 2011.

[13] B. Yordanov, J. Kim, R. L. Petersen, A. Shudy, V. V. Kulkarni, and A. Phillips, "Computational design of nucleic acid feedback control circuits," *ACS Synth. Biol.*, vol. 3, no. 8, pp. 600–616, Aug. 2014.

[14] D. Soloveichik, G. Seelig, and E. Winfree, "DNA as a universal substrate for chemical kinetics," *Proc. Nat. Acad. Sci. USA*, vol. 107, no. 12, pp. 5393–5398, Mar. 2010.

[15] K. Miyakawa, T. Okano, and S. Yamazaki, "Cluster synchronization in a chemical oscillator network with adaptive coupling," *J. Phys. Soc. Jpn.*, vol. 82, no. 3, p. 034005, Mar. 2013.

[16] N. J. Jiang, X. Y. Liu, W. W. Yu, and J. Shen, "Finite-time stochastic synchronization of genetic regulatory networks," *Neurocomputing*, vol. 167, pp. 314–321, Nov. 2015.

[17] P. Fries, J. H. Reynolds, A. E. Rorie, and R. Desimone, "Modulation of oscillatory neuronal synchronization by selective visual attention," *Science*, vol. 291, no. 5508, pp. 1560–1563, Feb. 2001.

[18] A. Arenas, A. Díaz-Guilera, J. Kurths, Y. Moreno, and C. Zhou, "Synchronization in complex networks," *Phys. Rep.*, vol. 469, no. 3, pp. 93–153, Dec. 2008.

[19] A. Alofi, F. L. Ren, A. Al-Mazrooei, A. Elaiw, and J. D. Cao, "Power-rate synchronization of coupled genetic oscillators with unbounded time-varying delay," *Cognit. Neurodyn.*, vol. 9, no. 5, pp. 549–559, Oct. 2015.
[20] L. X. Yang and J. Jiang, "Impacts of link addition and removal on synchronization of an elementary power network," *Physica A, Stat. Mech. Appl.*, vol. 479, pp. 99–107, Aug. 2017.
[21] D. Meng and Y. M. Li, "Adaptive synchronization of 4-dimensional energy resource unknown time-varying delay systems," *IEEE Access*, vol. 5, pp. 21258–21263, 2017.
[22] Y. Y. Wang, Y. X. Zhu, H. R. Karimi, and X. H. Li, "Sampled-data exponential synchronization of chaotic Luri'e systems," *IEEE Access*, vol. 5, pp. 17834–17840, 2017.
[23] A. El-Keyi, O. Ureten, H. Yanikomeroglu, and T. Yensen, "LTE for public safety networks: Synchronization in the presence of jamming," *IEEE Access*, vol. 5, pp. 20800–20813, 2017.
[24] Z. Nie, P. F. Wang, C. Tian, and C. D. Mao, "Synchronization of two assembly processes to build responsive DNA nanostructures," *Angewandte Chemie Int. Ed.*, vol. 53, no. 32, pp. 8402–8405, Aug. 2014.
[25] D. Halicka, H. Zhao, J. W. Li, J. Garcia, M. Podhorecka, and Z. Darzynkiewicz, "DNA damage response resulting from replication stress induced by synchronization of cells by inhibitors of DNA replication: Analysis by flow cytometry," in *Cell Cycle Synchronization* (Methods in Molecular Biology), vol. 1524, G. Banfalvi, Ed. New York, NY, USA: Humana Press, 2017, pp. 107–119.
[26] D. J. Ferullo, D. L. Cooper, H. R. Moore, and S. T. Lovett, "Cell cycle synchronization of *Escherichia coli* using the stringent response, with fluorescence labeling assays for DNA content and replication," *Methods*, vol. 48, no. 1, pp. 8–13, May 2009.
[27] G. H. Li, "Modified projective synchronization of chaotic system," *Chaos Solitons, Fractals*, vol. 32, no. 5, pp. 1786–1790, Jun. 2007.
[28] C. Y. Chen and D. L. Xu, "Secure digital communication using controlled projective synchronisation of chaos," *Chaos Solitons, Fract.*, vol. 23, no. 3, pp. 1063–1070, Feb. 2005.
[29] H. Pu, Y. Z. Li, C. X. Ma, and H. B. Mu, "Analysis of the projective synchronization of the urban public transportation super network," *Adv. Mech. Eng.*, vol. 9, no. 6, Jun. 2017.
[30] Y. Lei, L. Zhang, Y. Wang, and Y. Fan, "Generalized matrix projective outer synchronization of non-dissipatively coupled time-varying complex dynamical networks with nonlinear coupling functions," *Neurocomputing*, vol. 230, pp. 390–396, May 2017.

CHENGYE ZOU received the B.S. degree in physics and the M.E. degree in theoretical physics from Liaoning Normal University, Dalian, China. He is currently pursuing the Ph.D. degree with the Dalian University of Technology, Dalian. His research interests include biological computing and its applications.

XIAOPENG WEI is currently a Professor with the Dalian University of Technology, Dalian, China. He has (co-)authored about 160 papers published. His research interests include computer animation and intelligent CAD.

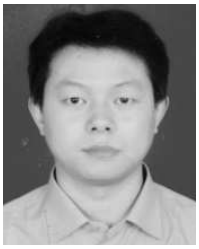

QIANG ZHANG received the Ph.D. degree from Xidian University, Xi'an, China, in 2002. He is currently a Professor with the Dalian University of Technology, Dalian, China. He is also a Professor with Dalian University, Dalian. His research interests include intelligent computing and intelligent robots. He has served on the editorial boards of seven international journals and has edited special issues in journals, such as *Neurocomputing* and the *International Journal of Computer Applications in Technology*.

YUAN LIU is currently pursuing the Ph.D. degree with the Dalian University of Technology, Dalian, China. His research interests include biological computing and its applications.